RESEARCH PAPERS

Acta Cryst. (1997). B53, 739–744

Electron Density in $YTiO_3$

J. R. HESTER,[a]* K. TOMIMOTO,[b] H. NOMA,[b] F. P. OKAMURA[a] AND J. AKIMITSU[b]

[a]*National Institute for Research in Inorganic Materials, Namiki 1-1, Tsukuba, Ibaraki 305, Japan, and* [b]*Department of Physics, Aoyama, Gakuin University, 6-16-1 Chitosedai, Setagaya, Tokyo 157, Japan. E-mail: jrh@nirim.go.jp*

(*Received 4 September 1996; accepted 10 April 1997*)

Abstract

Accurate electron density analyses have been performed on the title compound, yttrium titanate, at room and low temperature using W $K\alpha$ radiation. Room- and low-temperature $\Delta\rho$ maps are generally consistent. Difference electron densities near the two symmetrically independent O atoms differ markedly. These observations may have significance for understanding the role of the O atom in mediating *d*-electron interactions between neighbouring Ti coordination polyhedra. Features having lower symmetry than that of the approximately octahedral local environment are observed within the Ti coordination octahedron. Crystal data at room temperature: $YTiO_3$, $M_r = 184.79$, $T = 293$ K, *Pnma*, $a = 5.6901(4)$, $b = 7.6130(7)$, $c = 5.3381(6)$ Å, $V = 231.24(4)$ Å^3, $Z = 4$, $D_x = 5.308$ Mg m^{-3}, μ(W $K\alpha$) = 1.02 mm^{-1}, $R = 0.024$, $wR = 0.017$, $S = 1.64(2)$ for 2996 independent reflections. Low temperature: $T = 127$ K, *Pnma*, $a = 5.690(4)$, $b = 7.583(6)$, $c = 5.318(5)$ Å, $V = 229.5(3)$ Å^3, $D_x = 5.35$ Mg m^{-3}, μ(W $K\alpha$) = 1.02 mm^{-1}, $R = 0.021$, $wR = 0.015$, $S = 1.80(2)$ for 2968 independent reflections.

1. Introduction

$YTiO_3$ is a semiconductor at room temperature, becoming an insulating ferromagnet below 29 K. It obeys the Curie–Weiss law with a Curie constant characteristic of a spin-only d_1 system. The saturation moment of the ferromagnetic phase, 0.84 μ_B mol^{-1}, also suggests that a single *d* electron is localized at the Ti atom (Goral, Greedan & MacLean, 1982).

$YTiO_3$ is a member of the distorted perovskite family. MacLean, Ng & Greedan (1979) have reviewed the structures of the $RETiO_3$ family for *RE* = La, Nd, Sm, Gd and Y. The $YTiO_3$ structure has the smallest unit-cell volume of the series due to contraction of the *b* and *a* axes. The contraction of the *b* axis is associated with tilting of the Ti—O octahedron about the *a* axis; this tilting is of considerable interest as the Ti—O—Ti link is thought to mediate ferromagnetic ordering through a superexchange interaction. Fujitani & Asano (1995) have published band-structure calculations on $YTiO_3$ using the full-potential linear augmented plane wave method (FLAPW). Even though these calculations ignore the presumably strong electron correlation effects required by superexchange, the tilting of the interpolyhedral Ti—O—Ti angles is shown to minimize the calculated energy and to be a necessary condition for the existence of an insulative band gap.

Ordering of degenerate orbitals between neighbouring coordination polyhedra has been observed at low temperature in K_2CuF_4 (Ito & Akimitsu, 1976). Similar orbital ordering in $YTiO_3$ would lead to a reduction in symmetry from *Pnma* to $P2_1/c$, indications of which may be observable above the transition temperature. The present experiments aimed to image the Ti electron distribution above the transition temperature and, if possible, to observe any signs of orbital ordering in the experimental electron density.

2. Experimental

Single crystals of $YTiO_3$ were grown by the floating zone method in a reducing atmosphere (Ar/H_2 = 40/60). The starting material, of stoichiometry $YTiO_{2.90}$, was obtained by mixing powders of Ti, Y_2O_3 and TiO_2. After pressing the starting material into a rod and purging the sample atmosphere with Ar, the material was held in a vacuum for 12 h before commencing the growth operation. A black crystal of diameter 5 mm and length 20 mm was obtained. The sample was characterized by electron probe micro-analysis, polarizing microscopy, measurement of the temperature dependence of magnetization and thermogravimetric/differential thermal analysis. These measurements confirmed that the sample was an insulative ferromagnet, with $T_C = 30$ K, and that $|\delta|$ was ≤ 0.05 for the composition $YTiO_{3+\delta}$. The saturation magnetic moment agreed with the previously published value of 0.84 μ_B mol^{-1}. Small samples were cut from the crystal and ground into spheres using a new ball-milling technique (Takahashi, Yamamoto, Ohshima, Yukino & Okamura, 1996).

Details of sample preparation and characterization will be published elsewhere. A spherical sample of diameter 0.8 mm was used for all data collections. Such a large sample size was considered reasonable, given the approximately threefold decrease in X-ray wavelength compared with Ag or Mo sources and consequent weakening of both reflected intensity and extinction effects.

Three data collections were performed at two temperatures using unmonochromated white radiation from a tungsten target operating at 150 kV and 12 mA. Reflected radiation was collected using an energy-sensitive solid-state detector (Ge) mounted on the 2θ arm and the W $K\alpha_1$ line was then selected using a single channel analyser. For room-temperature data collections, accurate cell dimensions and corrections for diffractometer misalignment were obtained by the eight-setting method (King & Finger, 1979) using three reflections between $\theta = 4.5$ and 6.9°. At low temperature 23 reflections ($4.5 < \theta < 13.95°$) were used. The assignment of the *Pnma* space group was checked by analysis of systematically absent reflections. Zero intensities observed during scans around the scattering vector indicated that the significantly non-zero intensities observed at $\psi = 0°$ for some systematically absent reflections in space group *Pnma* were attributable to multiple scattering effects. Furthermore, the variation of intensity in the range $0 \leq \psi \leq 20°$ for the systematically absent 012 and 014 reflections coincided approximately with predictions for multiple scattering in the *Pnma* structure calculated using a slightly modified version of the program *IUANGLE* (Tanaka, Kumazawa, Tsubokawa, Maruno & Shirotani, 1994).

More than one complete hemisphere of data in reciprocal space was collected for each experiment using fixed-width θ scans. The scan width was not varied, as the energy-sensitive detector system completely filters the W $K\alpha_2$ line and thus peak width variation with 2θ angle becomes insignificant. Six standard reflections, collected after every 100 measurements, were used to correct for intensity fluctuations and were also used for calculation of an instability factor (McCandlish, Stout & Andrews, 1975). After absorption correction using A^* values for a sphere calculated by the method of Tibells (1982), and averaging equivalent reflections, Lorentz and polarization corrections were applied and least-squares refinement carried out using $w = 1/\sigma^2(F)$, assuming neutral harmonically vibrating spherically symmetric atoms and including a Zachariasen-type extinction parameter (Zachariasen, 1967). Reflections with $F > 0$ were used for parameter refinement. Data collection details are given in Table 1 and refined structural parameters are listed in Table 2. Refinement statistics were calculated for all reflections. All calculations were performed using *Xtal*3.4 (Hall, King & Stewart, 1995) running under a Unix operating system on an IBM compatible PC. Absorption coefficients were obtained from Sasaki (1990), and f' and f'' were taken from *International Tables for Crystallography* (Wilson, 1992).

The absorption and dispersion correction procedure for W $K\alpha$ radiation did not differ from that applied at longer wavelengths. However, special care was taken to check for multiple diffraction effects, by measuring complete sets of equivalent reflections. The low merging R factors for all data sets indicate that multiple reflection did not significantly affect the data. This conclusion was verified by inspection of poorly merged reflections and by multiple reflection modelling using *IUANGLE* (Tanaka, Kumazawa, Tsubokawa, Maruno & Shirotani, 1994). Extinction effects when white radiation is incident on the crystal do not differ from those for monochromatic radiation (Tomoyoshi, Yamada & Watanabe, 1980). Corrections for extinction were within the limits assumed by theory.

Data set 1 was collected soon after an earthquake-induced misalignment of the diffractometer. Part of this misalignment was corrected by the eight-setting procedure. The consistent results obtained indicate that serious systematic errors can be minimized by a sound experimental method. Data set 1 is included here to illustrate this point.

3. Structural parameters

The Y atom vibrates anisotropically, with U^{22} the largest. From the structural diagram (Fig. 1) it is clear that Y is more constrained by the two O1 atoms in the

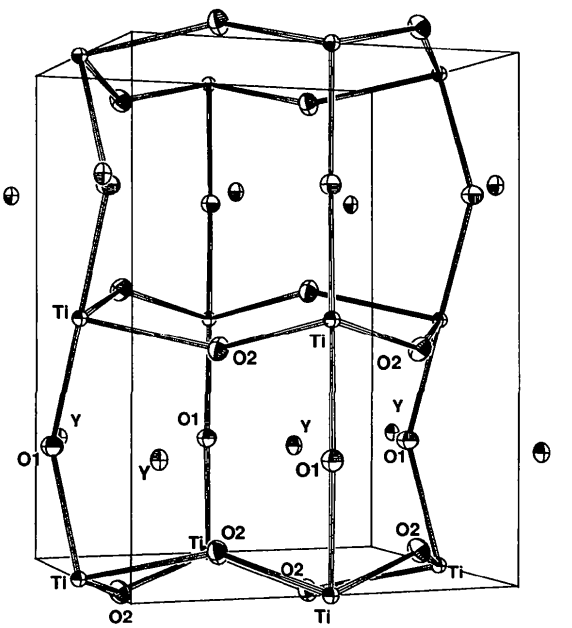

Fig. 1. Thermal ellipsoid plot of $YTiO_3$ unit cell, **b** axis vertical. Ellipsoids are plotted at the 90% probability level.

Table 1. *Experimental details*

	(1)	(2)	(3)
Crystal data			
Chemical formula	O_3TiY	O_3TiY	O_3TiY
Chemical formula weight	184.79	184.79	184.79
Cell setting	Orthorhombic	Orthorhombic	Orthorhombic
Space group	*Pnma*	*Pnma*	*Pnma*
a (Å)	5.6890 (10)	5.6901 (4)	5.690 (4)
b (Å)	7.6094 (9)	7.6130 (7)	7.583 (6)
c (Å)	5.3350 (8)	5.3381 (6)	5.318 (5)
V (Å^3)	230.95 (6)	231.24 (4)	229.5 (3)
Z	4	4	4
D_x (Mg m^{-3})	5.314	5.308	5.35
Radiation type	W $K\alpha$	W $K\alpha$	W $K\alpha$
Wavelength (Å)	0.21060	0.21060	0.21060
No. of reflections for cell parameters	3	3	23
θ range (°)	4.5–6.9	4.5–6.9	4.5–13.95
μ (mm^{-1})	1.02	1.02	1.02
Temperature (K)	293	293	127
Crystal form	Sphere	Sphere	Sphere
Crystal size (mm)	0.800 (diameter)	0.800 (diameter)	0.800 (diameter)
Crystal colour	Black	Black	Black
Data collection			
Diffractometer	Huber	Huber	Huber
Data collection method	θ scans	θ scans	θ scans
Absorption correction	Spherical (Tibballs, 1982)	Spherical (Tibballs, 1982)	Spherical (Tibballs, 1982)
T_{min}	0.310	0.310	0.310
T_{max}	0.314	0.322	0.316
No. of measured reflections	11 343	13 340	12 493
No. of independent reflections	1906	2996	2968
No. of observed reflections	1864	2898	2916
Criterion for observed reflections	$F > 0$	$F > 0$	$F > 0$
R_{int}	0.0304	0.0230	0.0248
θ_{max} (°)	15	25	17.7
Range of h, k, l	$-14 \rightarrow h \rightarrow 14$ $-21 \rightarrow k \rightarrow 21$ $-13 \rightarrow l \rightarrow 13$	$-22 \rightarrow h \rightarrow 16$ $-21 \rightarrow k \rightarrow 21$ $-15 \rightarrow l \rightarrow 15$	$-16 \rightarrow h \rightarrow 9$ $-21 \rightarrow k \rightarrow 21$ $-15 \rightarrow l \rightarrow 15$
No. of standard reflections	6	6	6
Frequency of standard reflections	Every 100 reflections	Every 100 reflections	Every 100 reflections
Refinement			
Refinement on	F	F	F
R	0.0017	0.0024	0.0021
wR	0.0013	0.0017	0.0015
S	2.27 (4)	1.64 (2)	1.80 (2)
No. of reflections used in refinement	1864	2898	2916
No. of parameters used	29	29	29
Weighting scheme	$w = 1/\sigma^2(F)$	$w = 1/\sigma^2(F)$	$w = 1/\sigma^2(F)$
$(\Delta/\sigma)_{max}$	0.0017	0.0016	0.0015
$\Delta\rho_{max}$ (e Å^{-3})	0.94	1.60	1.39
$\Delta\rho_{min}$ (e Å^{-3})	−1.20	−1.53	−1.66
Extinction method	Zachariasen (1967)	Zachariasen (1967)	Zachariasen (1967)
Extinction coefficient	y = 0.86	y = 0.84	y = 0.85
Source of atomic scattering factors	*International Tables for Crystallography* (1992, Vol. C)	*International Tables for Crystallography* (1992, Vol. C)	*International Tables for Crystallography* (1992, Vol. C)

$y = 1/4$ plane at distances of 2.230(2) and 2.3093(15) Å than by the closest O2 atoms in the $y \simeq 0$ plane at distances of 2.2758(11) and 2.5000(13) Å, indicating stronger net interactions between Y and O1.

The Ti-atom vibration is isotropic, in accordance with the approximately octahedral local environment, and comparison with the Y vibration parameters indicates that the Ti atom is considerably more constrained. Both O1 and O2 atoms vibrate more strongly perpendicular to the Ti—O bonds, as expected.

The Ti—O—Ti interaction may be important in mediating the magnetic interaction between Ti polyhedra. Two distinct Ti—O—Ti angles are present in the structure. At low temperature, the Ti—O1—Ti angle is 139.86(5)° and the Ti—O2—Ti angle is 143.54(3)°. At room temperature these angles are 140.18(3) and 143.58(2)°, respectively. The Ti—O1 and Ti—O2 bond lengths contract uniformly by 0.006 Å as the temperature is reduced. Room- and low-temperature values for the relevant bond lengths are, respectively (Å): Ti—O1, 2.0242(3), 2.018(1); Ti—O2, 2.0264(4), 2.020(1); Ti—O2′, 2.0803(4), 2.080(1), where a prime is used to distinguish the two symmetrically identical O2 atoms in the coordination octahedron.

Table 2. *Fractional atomic coordinates and equivalent isotropic displacement parameters (Å²)*

$U_{eq} = (1/3)\Sigma_i\Sigma_j U^{ij} a_i^* a_j^* \mathbf{a}_i.\mathbf{a}_j.$

	x	y	z
(1)			
Y	0.07341 (1)	1/4	0.97893 (1)
Ti	1/2	0.0	0.0
O1	0.4575 (1)	1/4	0.1209 (1)
O2	0.30941 (8)	0.05824 (7)	0.69028 (8)
(2)			
Y	0.07339 (1)	1/4	0.97895 (1)
Ti	1/2	0.0	0.0
O1	0.45736 (9)	1/4	0.1209 (1)
O2	0.30942 (6)	0.05824 (6)	0.69031 (7)
(3)			
Y	0.07439 (1)	1/4	0.97796 (1)
Ti	1/2	0.0	0.0
O1	0.45729 (9)	1/4	0.12192 (9)
O2	0.30980 (6)	0.05827 (5)	0.69019 (7)

4. Electron density

Difference electron densities were obtained by Fourier transformation of $F_o - F_c$ using all reflections with $\sin\theta/\lambda \leq 1.1$. The estimated average error in the electron density, $\sigma(\Delta\rho)$, defined as $(2/V^2)\Sigma_{1/2}\sigma^2(\Delta F)$ (Cruickshank, 1949), equalled 0.19 and 0.18 for room- (data set 2) and low-temperature syntheses, respectively. The $\Delta\rho$ features discussed below appear in all three Fourier syntheses, underlining the reliability of the present results. The low-temperature synthesis is presumed to be the most accurate and is used in the following discussion.†

4.1. *Ti coordination octahedron*

Three distinct Ti—O bond lengths are present in the distorted Ti coordination octahedron. The Ti—O1 bond links neighbouring Ti octahedra along the **b** axis, while the Ti—O2 bonds link octahedra within the **ac** plane. Fig. 2 shows strong electron density depletion along the long Ti—O2′ vector and lesser depletion along the short Ti—O2 vector. Both room-temperature maps show similar, but smaller, local minima in the same regions.

Local minima are also present further from the Ti nucleus along the bond bisector in both room- and low-temperature $\Delta\rho$. The symmetry of these minima does not reflect the approximate octahedral Ti coordination symmetry, in contrast to the minima closer to the Ti nucleus.

In the plane perpendicular to Fig. 2 (Fig. 3) the negative difference density is elongated in the direction of the O1 nucleus. There is some indication of asymmetric electron depletion away from the octahedral axes, similar to that observed for Fig. 2, however, room-temperature sections do not show this feature.

† Lists of structure factors and anisotropic displacement parameters, and room-temperature $\Delta\rho$ maps have been deposited with the IUCr (Reference: OA0005). Copies may be obtained through The Managing Editor, International Union of Crystallography, 5 Abbey Square, Chester CH1 2HU, England.

The two distinct Ti—O—Ti bonds have markedly different characters. Whereas electrons accumulate in a broad area of diffuse positive density around the O1 atom, no notable $\Delta\rho$ features are observed around the O2 atom (Figs. 2 and 3). These bonds may be compared with the strong covalent Ti—O bonds observed in $KTiOPO_4$ by Hansen, Protas & Marnier (1991). Ti—O bond lengths in the distorted Ti—O coordination

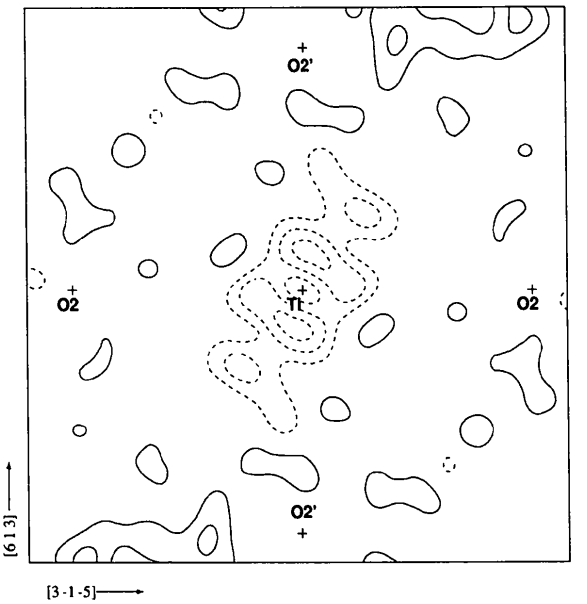

Fig. 2. $\Delta\rho$ in the plane of the Ti—O2 bonds at low temperature. The O2 atom terminating the longest Ti—O2 bond is primed. Contour interval 0.3 e Å^{-3}, solid lines positive $\Delta\rho$, dashed lines negative $\Delta\rho$. Borders 4.75 × 4.75 Å, boundary directions approximate.

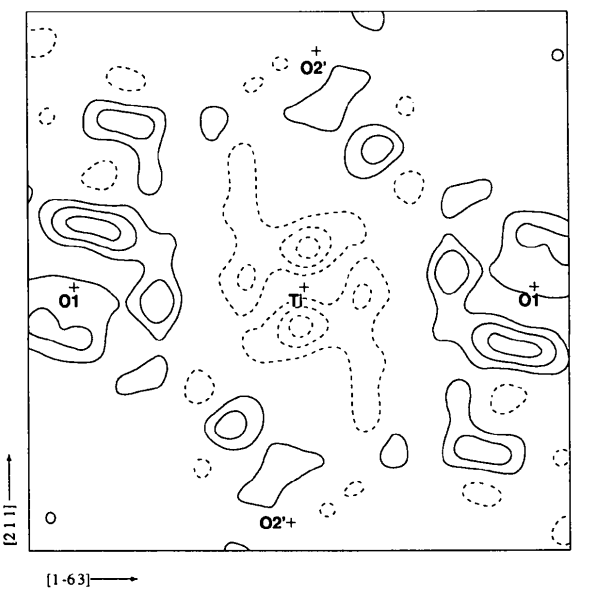

Fig. 3. $\Delta\rho$ in the Ti—O1—O2′ plane at low temperature. Contours and borders as in Fig. 2, boundary directions approximate.

octahedra in that structure lie between 1.72 and 2.15 Å, that is, the shortest bond lengths are considerably smaller than those observed here. Diffuse positive difference density was observed by those authors around O atoms with Ti—O bond lengths similar to those in the present structure. Although these densities are reminiscent of $\Delta\rho$ observed here, the details of the electron redistribution differ, as do the magnitudes of the electron accumulation around the O atoms.

Although the present Ti bonding configuration is distorted octahedral, octahedral behaviour provides a useful basis for analysis of the observed difference density. In an octahedral field, Ti *d* orbitals are expected to split into higher-energy e_g orbitals, oriented along the metal–ligand bonds, and t_{2g} orbitals, directed between the bonds. Loss of *d* electrons from a neutral atom, where all orbitals are equally occupied, should therefore produce greater depletion along the bonds, as we observe here. We expect less depletion in the t_{2g} direction, rather than difference density peaks. This can be seen by considering that, in the neutral Ti atom, each *d* orbital notionally contains 2/5 e. Removal of one *d* electron by first emptying the e_g orbitals gives a total t_{2g} orbital occupation of 1/3, less than the neutral atom occupation.

Thus, most features in the difference density distribution around Ti are explicable in terms of *d* orbital splitting in an octahedral field. However, the extra depletion along two of the Ti—O2 bond bisectors in Fig. 3 cannot be analysed in this way. It is not related solely to the Ti—O2 bonding geometry, as similar depletions would be expected along the other Ti—O2 bisectors. Neither is it obviously related to the disposition of Ti atoms in the second coordination sphere.

4.2. *Y electron density*

Redistribution of ρ around Y is rather complex and is best analysed in terms of the nearest-neighbour O atoms. Fig. 4, which is approximately parallel to the (101) plane, shows that two areas of strong depletion lie close to the Y nucleus. The geometry of these depletions suggests that they are related to interactions with the nearest-neighbour O atoms. The size of the depletions relative to one another agrees with the relative strength of the Y—O interactions deduced from the Y vibrational parameters, as the strongest depletion lies along the Y—O1 vector.

Due to the anisotropy of the Y environment, it is reasonable to suppose that anharmonic thermal vibrations could contribute to the observed $\Delta\rho$ maps. Comparison with the room-temperature maps shows that peaks around Y are sharper at low temperature. As this is not necessarily inconsistent with expectations based on anharmonicity (Restori & Schwarzenbach, 1996), no firm conclusions can be drawn.

Table 3. *Charges in e by Hirshfeld partitioning*

Data set	Y	Ti	O1	O2
(1)	0.48 (8)	0.85 (9)	−0.81 (1)	−0.5 (1)
(2)	0.45 (5)	1.14 (5)	−1.26 (3)	−0.39 (3)
(3)	0.48 (7)	1.00 (9)	−1.02 (9)	−0.49 (9)

5. Atomic charges

Charges assigned to nuclei using the partitioning scheme of Hirshfeld (1977) are presented in Table 3. Quite apart from any physical significance that may be contained in these figures, they provide a useful measure of the reproducibility of the charge-density results and are particularly sensitive to errors in the low-order structure factors. Charge values agree well with one another. The Y charge, +0.5, is remarkably reproducible. O1 is consistently more negative than O2, reflecting the greater accumulation of difference density observed around the former atom. Although caution is advisable in giving physical meaning to these charge estimates, theories of superexchange involve partial donation of an electron by the oxygen back to the metal atom, which would reduce the atomic polarities, in accordance with the present observations.

6. Discussion

The present experiments suggest that the Ti atom has lost a single *d* electron, predominantly from the e_g orbitals. There is no evidence of the loss of any *s* electrons. Diffuse positive difference density accumu-

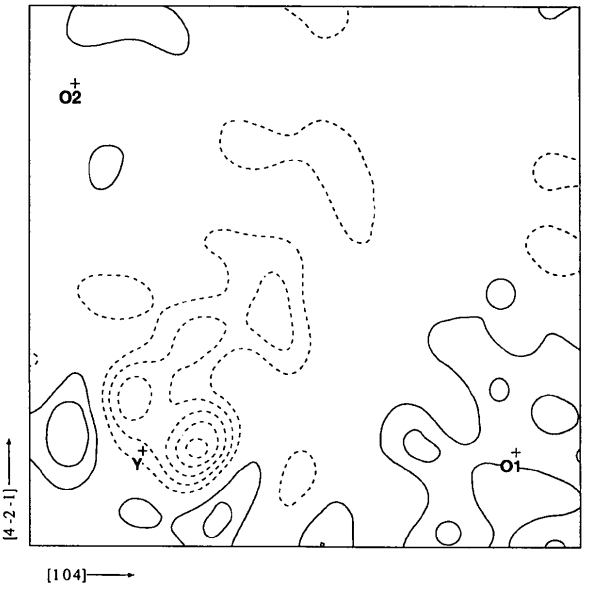

Fig. 4. Density along Y—O vectors. Contours as in previous figures. Borders 3.49 × 2.81 Å, boundary directions approximate.

lates in the region of O1, which shows clear signs of interaction with Y. This interaction is reflected by depleted electron density along the Y—O1 vector, which may indicate anharmonic vibration due to strong O1—Y repulsion, and by greater thermal vibration of the Y atom out of the plane of the Y—O1 vectors.

These conclusions are in good agreement with both experiment and theory. Magnetic measurements predict $1d$ electron per Ti atom and elementary crystal field theory predicts that the e_g orbitals oriented along the bonds will have higher energy than the t_{2g} set. The presence of a significant Y—O1 interaction is implied by the results of Zubkov, Berger, Artamonova & Bazuev (1984), who found that the shortest Y/La—O1 distance varies atypically at the onset of ferromagnetic behaviour ($x = 0.6$) in compounds in the series $Y_xLa_{1-x}TiO_3$.

The Ti—O—Ti bond is thought to mediate interaction between the unpaired Ti d electrons, leading to ferromagnetism at low temperatures. It is clear from the $\Delta\rho$ maps that the two Ti—O bonds have distinct characters and that a significant Y—O1 interaction exists. The Ti—O1—Ti bond angle is smaller by 0.22° at low temperature, whereas the Ti—O2—Ti angle changes by only 0.04°. We therefore speculate that the onset of ferromagnetism is linked to strengthening of Ti—O1—Ti superexchange, perhaps through overlap of hybridized Ti t_{2g} orbitals with O1 sp^3 hybrid orbitals. The degree of O1 hybridization may be sensitive to the Y—O1 distance.

The authors are very grateful to Mr Takeyoshi Takaoka for providing the crystals, and to Professor T. Arima (Tsukuba University) and Professor Y. Tokura (University of Tokyo). They also wish to thank Mr Y. Takahashi for help in preparing spherical specimens and for valuable discussions, and Dr K. Tanaka for kindly providing a copy of the program *IUANGLE*. JH wishes to thank the Science and Technology Agency of Japan for providing a fellowship which allowed this work to be carried out.

References

Cruickshank, D. W. J. (1949). *Acta Cryst.* **2**, 65–82.

Fujitani, H. & Asano, S. (1995). *Phys Rev. B*, **51**, 2098–2102.

Goral, J. P., Greedan, J. E. & MacLean, D. A. (1982). *J. Solid State Chem.* **43**, 244–250.

Hall, S. R., King, G. S. D. & Stewart, J. M. (1995). Editors. *Xtal*3.4 *Reference Manual*. Perth: Lamb Printers.

Hansen, N. K., Protas, J. & Marnier, G. (1991). *Acta Cryst.* B**47**, 660–672.

Hirshfeld, F. L. (1977). *Isr. J. Chem.* **16**, 198–201.

Ito, Y. & Akimitsu, U. (1976). *J. Phys. Soc. Jpn*, **40**, 1333–1338.

King, H. E. & Finger, L. W. (1979). *J. Appl. Cryst.* **12**, 374–378.

MacLean, D. A., Ng, H.-N. & Greedan, J. E. (1979). *J. Solid State Chem.* **30**, 35–44.

McCandlish, L. E., Stout, G. H. & Andrews, L. C. (1975). *Acta Cryst.* A**31**, 245–249.

Restori, R. & Schwarzenbach, D. (1996). *Acta Cryst.* A**52**, 369–378.

Sasaki, S. (1990). *X-ray Absorption Coefficients of the Elements (Li to Bi, U)*. Technical Report 90-16. National Laboratory for High Energy Physics, 1-1 Oho, Tsukuba-shi, Ibaraki 305, Japan.

Takahashi, Y., Yamamoto, K., Ohshima, K., Yukino, K. & Okamura, F. P. (1996). *J. Appl. Cryst.* **29**, 206–207.

Tanaka, K., Kumuzawa, S., Tsubokawa, M., Maruno, S. & Shirotani, I. (1994). *Acta Cryst.* A**50**, 246–252.

Tibballs, J. E. (1982). *Acta Cryst.* A**38**, 161–163.

Tomoyoshi, S., Yamada, M. & Watanabe, H. (1980). *Acta Cryst.* A**36**, 600–604.

Zachariasen, W. H. (1967). *Acta Cryst.* **23**, 558–564.

Zubkov, V. G., Berger, I. F., Artamonova, A. M. & Bazuev, G. V. (1984). *Sov. Phys. Crystallogr.* **29**, 296–297.